

On chip chiral and plasmonic hybrid dimer or tetramer: Generic way to reverse longitudinal and lateral optical binding forces

Sudipta Biswas[†], Roksana Khanam Rumi[†], Tasnia Rahman Raima[†], Saikat Chandra Das[†], and M R C Mahdy[‡]

Citation: Chin. Phys. B, 2022, 31 (**5**): 054202. DOI: 10.1088/1674-1056/ac322d
Journal homepage: http://cpb.iphy.ac.cn; http://iopscience.iop.org/cpb

What follows is a list of articles you may be interested in

Graphene-tuned threshold gain to achieve optical pulling force on microparticle

Hong-Li Chen(陈鸿莉) and Yang Huang(黄杨)
Chin. Phys. B, 2021, 30 (**6**): 064205. DOI: 10.1088/1674-1056/abd9b4

Broadband absorption enhancement with ultrathin MoS_2 film in the visible regime

Jun Wu(吴俊)
Chin. Phys. B, 2021, 30 (**2**): 024208. DOI: 10.1088/1674-1056/abc3b5

Variable optical chirality in atomic assisted microcavity

Hao Zhang(张浩), Wen-Xiu Li (李文秀), Peng Han(韩鹏), Xiao-Yang Chang(常晓阳), Shuo Jiang(蒋硕), An-Ping Huang(黄安平), and Zhi-Song Xiao(肖志松)
Chin. Phys. B, 2020, 29 (**11**): 114207. DOI: 10.1088/1674-1056/abb660

Geometrical condition for observing Talbot effect in plasmonics infinite metallic groove arrays

Afshari-Bavil Mehdi, Xiao-Ping Lou(娄小平), Ming-Li Dong(董明利), Chuan-Bo Li(李传波), Shuai Feng(冯帅), Parsa Saviz, Lian-Qing Zhu(祝连庆)
Chin. Phys. B, 2018, 27 (**12**): 124204. DOI: 10.1088/1674-1056/27/12/124204

Silicon nanophotonics for on-chip light manipulation

Jingshu Guo(郭敬书), Daoxin Dai(戴道锌)
Chin. Phys. B, 2018, 27 (**10**): 104208. DOI: 10.1088/1674-1056/27/10/104208

On chip chiral and plasmonic hybrid dimer or tetramer: Generic way to reverse longitudinal and lateral optical binding forces

Sudipta Biswas[†], Roksana Khanam Rumi[†], Tasnia Rahman Raima[†], Saikat Chandra Das[†], and M R C Mahdy[‡]

Department of Electrical & Computer Engineering, North South University, Bashundhara, Dhaka, 1229, Bangladesh

(Received 4 September 2021; revised manuscript received 7 October 2021; accepted manuscript online 22 October 2021)

For both the longitudinal binding force and the lateral binding force, a generic way of controlling the mutual attraction and repulsion (usually referred to as reversal of optical binding force) between chiral and plasmonic hybrid dimers or tetramers has not been reported so far. In this paper, by using a simple plane wave and an onchip configuration, we propose a possible generic way to control the binding force for such hybrid objects in both the near-field region and the far-field region. We also investigate different inter-particle distances while varying the wavelengths of light for each inter-particle distance throughout the investigations. First of all, for the case of longitudinal binding force, we find that chiral-plasmonic hybrid dimer pairs do not exhibit any reversal of optical binding force in the near-field region nor in the far-field region when the wavelength of light is varied in an air medium. However, when the same hybrid system of nanoparticles is placed over a plasmonic substrate, a possible chip, it is possible to achieve a reversal of the longitudinal optical binding force. Later, for the case of lateral optical binding force, we investigate a setup where we place the chiral and plasmonic tetramers on a plasmonic substrate by using two chiral nanoparticles and two plasmonic nanoparticles, with the setup illuminated by a circularly polarized plane wave. By applying the left-handed and the right-handed circular polarization state of light, we also observe the near-field and the far-field reversal of lateral optical binding force for both cases. As far as we know, so far, no work has been reported in the literature on the generic way of reversing the longitudinal optical binding force and the lateral optical binding force of such hybrid objects. Such a generic way of controlling optical binding forces can have important applications in different fields of science and technology in the near future.

Keywords: longitudinal binding force, plasmonics, chirality, optical force

PACS: 42.25.Bs, 42.25.Dd, 42.25.Gy, 42.25.Ja **DOI:** 10.1088/1674-1056/ac322d

1. Introduction

Particles can be accelerated or trapped by the transverse spatial gradient wave when irradiated with a laser beam.[1] Arthur *et al*. demonstrated the applications of such phenomena based on a series of notable experiments in the 1970s, and since then, optical manipulation has inspired many investigations of and applications in various particles, ranging from cold atoms to living cells.[2–4] Light can exert a radiation pressure on any object when they encounter each other, resulting in an optical force capable of manipulating particles.[5] A significant property of electromagnetic (EM) wave is that it can carry and transfer momentum. When a particle absorbs or scatters light, momentum is transferred from the light to the particle, causing it to move. It is typically believed that light can drive a particle forward; in fact, an incident plane wave with a photon momentum hk can carry a particle in the direction of k, independent of the particle properties.[5] Hence, light can be used in this way to control (or manipulate) particle movement, whenever a particle absorbs or scatters light and moves in the direction of the incident wave, we call it optical pushing force and if it travels against it, we call it optical pulling force.

In the field of optical manipulation, a relatively new member is optical binding force. The optical manipulations based on curl, gradient, and scattering forces have been investigated quite extensively within the areas of biological science,[6] physics,[1,7,8] and chemistry,[9] since its first observation in 1989, and the optical binding force has attracted much less attention comparatively.[10] As a result, perhaps the optical binding force is neither well defined nor clearly understood and still remains relatively unexplored in the broad field of optical micromanipulation.[11] The optical binding force can be defined as the induced interaction among optically bound particles when kept in an intense optical field.[4,10–12] It may also be classically described as an interaction of individual particles with the electromagnetic fields generated in other particles by light scattering process and optical rectification process.[4] In recent investigations, the optical binding force has been mainly in focus[13–24] and has also increasingly been favored as a tool for the optical manipulation of particles. Many optically induced arrays and configurations have been experimentally observed so far.[4,22,24–26]

Positive values of optical binding force mean that the force is attractive, while negative values refer to the fact that it is repulsive. Since optical binding force is not necessarily attractive at all times, it can be a very efficient tool to control the mutual attraction and repulsion among optically bound nanoparticles precisely for particle aggregation, crystallization, self-assembly, *etc*.[4,11,12,27,28] When a change or

[†]These authors contributed equally to this work.

[‡]Corresponding author. E-mail: mahdy.chowdhury@northsouth.edu

© 2022 Chinese Physical Society and IOP Publishing Ltd

adjustment in attraction and repulsion between closely adjacent nanodimers is observed, the phenomenon is known as the reversal of optical binding force. The work related to this novel area is even newer than some of the recent popular regions in optical manipulation, including the reversal of optical scattering force or passive tractor beams,[29–31] active tractor beams,[32] and optical lateral forces.[28,33–35]

We can classify the optical binding force[1,28,33,36–39] as two categories in terms of the inter-particle distances: a far-field optical binding force[36,39–42] and a near-field optical binding force.[33,38,43–46] When objects are placed at a distance nearly a micrometer or more apart, the optical binding force is defined as far-field one. A near-field optical binding force, on the other hand, can be defined for objects that are usually placed at a distance of 10 nm–250 nm apart.[11,28] So far, most of the researches on the optical binding force have focused on 'far-field optical manipulation'. In contrast, only a small number of researches have investigated the control of 'near-field optical binding force'; these being particularly between plasmonic dimers.[28,42–48] The optical binding force between chiral objects or similar matters[12,49,50] has received much less attention, except in a few researches.[12,49–54] Among these reports, even fewer researches have reported the "reversal of near-field optical binding force" for plasmonic dimers.[28,42–45,47,48] Notably, only a small number of investigations have been conducted on controlling the reversal of the optical binding force of chiral-plasmonic heterodimer sets.[12] Furthermore, the behavior of near-field optical force for chiral-plasmonic tetramers (4 nanoparticle sets) when shined by different polarization states of incident light and the effect of substrate on the simultaneous reversal of near-field optical binding force, have not been studied in the literature at all.

An effective method of integrating optics into nanotechnology and nanoscience is plasmonics. It deals with the collective oscillations of conduction electrons of plasmas.[12,28] Optical force of any plasmonic object generally arises from the surface force/polarization induced charges.[28,47,55,56] A chiral object or system, on the other hand, is one whose identical representation, regardless of orientation, cannot be superimposed on itself.[12] The chirality is omnipresent and essential for the proper functioning of key biological and physiological processes. Chiral bio-nano science has become a popular research field in recent decades due to the high selectivity for chiral biomolecules in biological systems.[57] The chiral structures include proteins and DNA/RNA, as well as a wide variety of medicines.[12,58,59]

In this work, we demonstrate that when a linearly polarized plane wave is propagating toward the "$+y$" direction hitting the plasmonic nanoparticle first or "$-y$" direction coming into contact with the chiral nanoparticle first with its polarization in the "x" direction of a plasmonic-chiral heterodimer set, the reversal of longitudinal optical binding force does not occur naturally even when the wavelength of light is varied. Next, we find a solution to this problem and show that when a heterodimer pair is positioned over a plasmonic substrate/chip, it is possible to control the reversal of longitudinal optical binding force for the near-field region and the far-field region.

Furthermore, we demonstrate that the reversal of lateral optical binding force for chiral-plasmonic tetramers for the near-field and for the far-field are possible when placed over a plasmonic substrate/chip and illuminated by the circularly polarized light propagating along the "$-z$" direction. The reversals are observed both for the right-handed circular polarization (RHCP) state of light and for left-handed circular polarization (LHCP) state of light. Compared with other researches in the past decade, the observations are quite new. Only a few researches have been conducted to control the reversals of optical binding force for chiral-plasmonic hybrid dimers set in both in the near-field region and in the far-field region.[12] To the best of our knowledge, no work has been reported on the reversal of longitudinal optical binding force for chiral and plasmonic hybrid dimers, and neither is the work on the reversal of lateral optical binding force for chiral and plasmonic tetramer layout. The detailed physics behind such reversals of the forces is discussed with the help of induced charges and current profiles due to the presence of a plasmonic chip. Notably, the induced charges on both the plasmonic particles and chiral nanoparticles play an important role in the total optical binding force both in the near-field region and in the far-field region.

2. Optical setups

We demonstrate a generic method to control the reversals of both the near and far-field longitudinal and lateral optical binding force when chiral and plasmonic nanoparticles are placed above a plasmonic substrate. In this paper, a set of configurations is studied which provides our proposed method of getting a reversal of longitudinal optical binding force. The schematic diagrams of our setups are given in Figs. 1(a)–1(d). The plasmonic-chiral heterodimer sets, with and without a plasmonic substrate placed underneath are used. The plasmonic and chiral spheres' radii are kept at $r = 100$ nm in all the configurations. The real part and imaginary part of permittivity of gold are cited from the standard Palik data. For the chiral nanoparticle, the refractive index is considered to be 1.45, and the chirality parameter is set to be $k = +1$. Using a radius size of 100 nm makes the experiments simple and does not exaggerate the simulation software because the small particles' resonance is not too strong. The COMSOL Multiphysics 5.3a is used to do all of the optical simulations (The details are given in the "Full Wave Simulation Set-up" section). We use the linearly polarized plane waves propagating in two directions in our setups and change the wavelength (λ) of the incident plane wave from 400 nm to 1200 nm. The light under investigation propagates towards the "$-y$" direction and

the "$+y$" direction and polarized along the "x" direction. The separation between the bottom of the spheres and the top surface of the substrate, *i.e.*, between dimers and tetramers is set to be 5 nm. All of these investigations are conducted in the air medium.

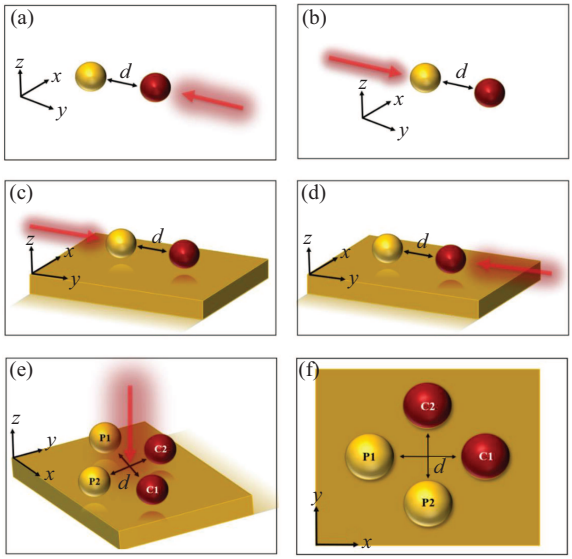


Fig. 1. (a) The "x"-polarized plane wave propagating in the "$-y$" direction towards a plasmonic nanoparticle (left) and a chiral (right) heterodimer nanoparticle with radius $r = 100$ nm placed in an air medium where the spheres' interparticle distance is d. (b) The same configuration as that in panel (a) with the polarized plane wave propagating in the "$+y$" direction. (c) The same configuration and direction of light as those in panel (b) with a plasmonic substrate under the nanospheres. (d) The same configuration as that in panel (c) with polarized plane wave propagating toward "$-y$" direction (left sphere is plasmonic and right sphere is chiral in panels (a)–(d)). (e) Circularly polarized incident plane wave propagating toward the "$-z$" direction among equidistant chiral — plasmonic tetramers (two chiral nanoparticles in maroon color, and two plasmonic nanoparticles in gold color, interparticle distance d placed over a plasmonic substrate. (f) The same chiral — plasmonic tetramers setup as those in panel (e), shown from the top view along the "x" axis and "y" axis.

Figure 1(a) shows our first setup where a plasmonic particle and a chiral nanoparticle are placed together. We keep the plasmonic sphere on the left while the chiral one is placed on the right side. The linearly polarized plane wave encounters the plasmonic nanoparticle first while propagating along the "$+y$" direction. Figure 1(b) shows the same configuration, but the direction of the incident plane wave is now propagating along the "$-y$" direction, coming into contact with the chiral nanoparticle first. In Fig. 1(c), the same two nanoparticles are placed over a plasmonic (gold) substrate. This time, we illuminate the setup with a linearly polarized light propagating along the "$+y$" direction, hitting the plasmonic nanoparticle first. In Fig. 1(d), we use the same configuration as that in Fig. 1(c), but in this case, we change the direction of the plane-polarized light that propagates in the "$-y$" direction illuminating the chiral nanoparticle first. Figure 1(e) shows an arrangement of a tetramers setup consisting of two plasmonic nanospheres and two chiral nanospheres kept at a height of 5 nm above a plasmonic (gold) substrate. Here, the interparticle distances are d_x (distance along the "x" axis) and d_y (interparticle distance along the "y" axis), respectively, where $d_x = d_y$. For each setup, we take a different interparticle distance between 200 nm and 2000 nm as done earlier, and change the wavelength of light for each distance. The chirality parameter for the setup when we use the RHCP state of plane wave is set to be $\kappa = -1$ but changed into $\kappa = +1$ for the LHCP state. The circular polarization gives a more conclusive result than linearly polarized light to control the mutual attraction and repulsion of near-field and far-field optical binding force for tetramers.

3. Theory

As stated above, in our proposed arrangement, we keep the chiral nanoparticle (named nanoparticle (i) on the right side and the plasmonic nanoparticle (called nanoparticle, (ii) on the left as shown in Figs. 1(a)–1(d). A commercial software "COMSOL Multiphysics" is used to calculate the optical force from the outside of the volume of these nanoparticles. referred to as "exterior" or "outside" optical force. The background field of the scatterer of radius 'a' is used to calculate the 'outside optical force' through using the time-averaged Minkowski stress tensor[12,33,60–62] at $r = a^+$:

$$\langle F^{\text{out}}_{\text{total}} \rangle = \oint \langle T^{\text{out}} \rangle \, \mathrm{d}s, \tag{1}$$

where

$$\langle T^{\text{out}} \rangle = \frac{1}{2} \text{Re} \left[D_{\text{out}} E^*_{\text{out}} + B_{\text{out}} H^*_{\text{out}} - \frac{1}{2} \bar{\bar{I}} \left(E^*_{\text{out}} \cdot D_{\text{out}} + H^*_{\text{out}} \cdot B_{\text{out}} \right) \right].$$

Here, subscript "out" represents the total exterior field of the scatterer (a combination of both the incident field and the scattered field); $\boldsymbol{E}$, $\boldsymbol{D}$, $\boldsymbol{H}$, and $\boldsymbol{B}$ denote the electric fields, the displacement vector, the magnetic field, and the induction magnetic field vectors, respectively. On the other hand, $\langle\ \rangle$ refers to the time average and $\bar{\bar{I}}$ the unity tensor.

For the plasmonic-chiral heterodimers, the longitudinal optical binding force is defined as $F_{\text{bind}(y)} = (F_{1(y)} - F_{2(y)})$. The positive value of the optical binding force represents an attractive optical binding force, while the negative value refers to a repulsive optical binding force. Here subscripts (y), 1, and 2 indicate the "y" component of optical binding force, the right sphere, the left sphere, respectively. Throughout this paper, these forces represent the face–to–face (F–F) optical binding forces.

For the chiral-plasmonic tetramer configuration, the lat-

eral binding force and the medial binding force are denoted by two resultant force components: $F_{C_1,P_1[\text{bind}(x)]} = F_{C_1(x)} - F_{P_1(x)}$ and $F_{C_2,P_2[\text{bind}(y)]} = F_{C_2(y)} - F_{P_2(y)}$. Here, C_1, C_2, P_1, and P_2 represent the first chiral nanoparticle (placed along the "x" axis), the second chiral nanoparticle (placed along the "y" axis), and the first plasmonic nanoparticle (placed along the "x" axis), and the second plasmonic nanoparticle (placed along the "y" axis), respectively. The positive value of the optical binding force $F_{C_1,P_1[\text{bind}(x)]}$ or $F_{C_2,P_2[\text{bind}(y)]}$ represents an attractive optical binding force, and the negative value refers to a repulsive optical binding force. Here subscripts (x) and (y) denote the positive "x" component of optical binding force and the positive "y" component of optical binding force, respectively.

For chiral nanoparticles used in this work, the fundamental relations are given by the following constitutive relation[5,12,63,64]

$$[D \;\; B] = \begin{bmatrix} \varepsilon_r\varepsilon_0 & \frac{i\kappa}{c} \\ \frac{i\kappa}{c} & \mu_r\mu_0 \end{bmatrix} [E \;\; H]. \tag{2}$$

Here, ε_r and μ_r represent the relative permittivity and permeability of the chiral material, respectively. The chirality parameter is denoted by κ, which is controlled by the inequality $\kappa < \varepsilon_r\mu_r$.[12] Furthermore ε_0 and μ_0 and care the permittivity, permeability, and speed of light in vacuum. The real part and the imaginary part of the permittivity of gold are taken from the standard Palik data for the plasmonic object.

4. Results and discussion

This paper aims to find and control the reversal of longitudinal optical binding force in the near-field region and far-field region for a plasmonic-chiral heterodimer setup by shining a linearly polarized plane wave on the dimers. The light shines towards the "$-y$" direction, coming into contact with the chiral nanoparticle first or "$+y$" direction, hitting the plasmonic nanoparticle first having polarization along the "x" direction.

4.1. Plasmonic and chiral hybrid heterodimers without substrate: No 'direct' reversal of longitudinal optical binding force

First, we investigate the reversal of optical binding force for plasmonic-chiral heterodimers in an air medium as shown in Figs. 1(a) and 1(b). We observe that the the configuration remains unchanged when changing the propagation direction of the incident light. Also, figure 2(a) shows the optical binding force when light propagates in the "$-y$" direction. Figures 2(b)–2(d) show that the longitudinal optical binding forces for the interparticle distance (d) values between 200 nm and 2000 nm. In this case, the incident electromagnetic (EM) wave propagate towards the "$-y$" direction coming into contact with the chiral nanoparticle first. The wavelength (λ) of the light varies from 400 nm to 1200 nm for each interparticle distance. Figures 2(b)–2(d) show that the optical binding forces are both repulsive for the near-field region and the far-field region. Therefore, no reversal of optical binding force is observed.

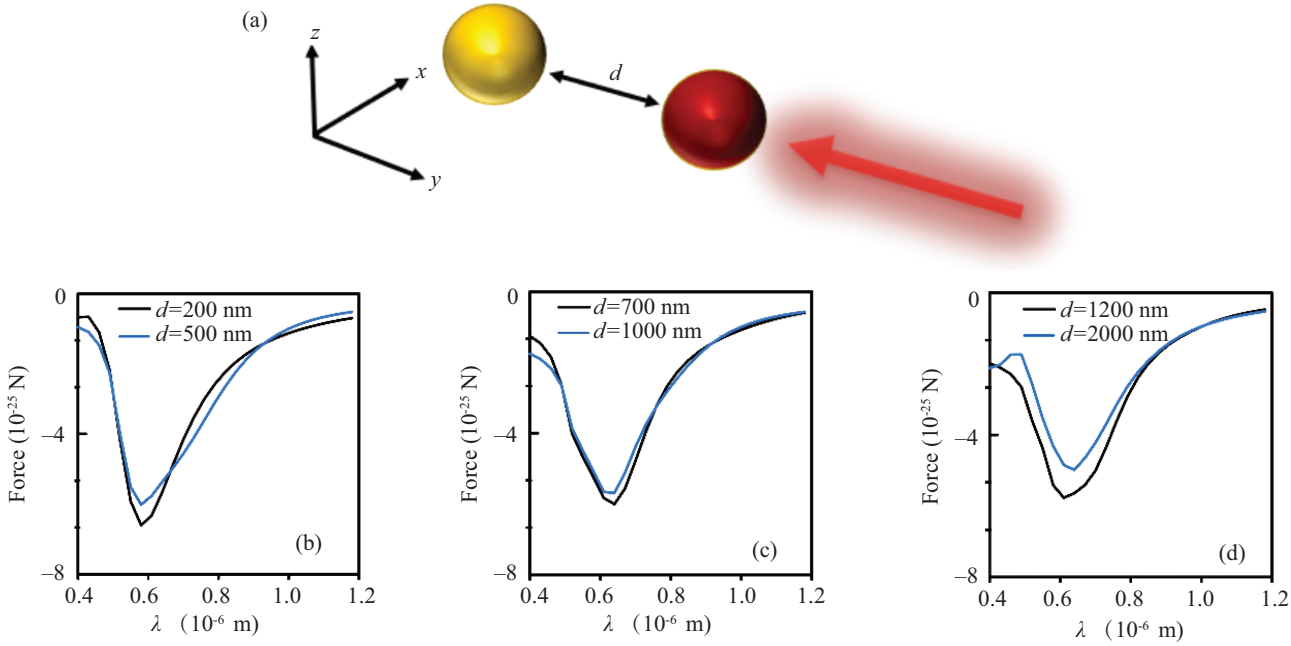


Fig. 2. The "x"-polarized plane wave propagating in the "$-y$" direction towards chiral (right) and plasmonic (left) heterodimer nanoparticles, where the spheres' interparticle distance is d and the wavelength is varied from 400 nm to 1200 nm in all cases. (a) A chiral and a plasmonic sphere (radius, $r = 100$ nm) are placed in air medium and their inter-particle gap distance is d. (b) The optical binding forces (along the "y" axis) are shown between the two hybrid dimers, for gap distances 200 nm and 500 nm by varying wavelength. (c) Optical binding forces $F_{\text{bind}(y)}$ are shown between the heterodimers, for gap distances 700 nm and 1000 nm by varying wavelength. (d) Optical binding forces for the same setup for $d = 200$ nm and 2000 nm are shown. (b)–(d) Repulsive optical binding forces (left sphere is plasmonic and right sphere is chiral).

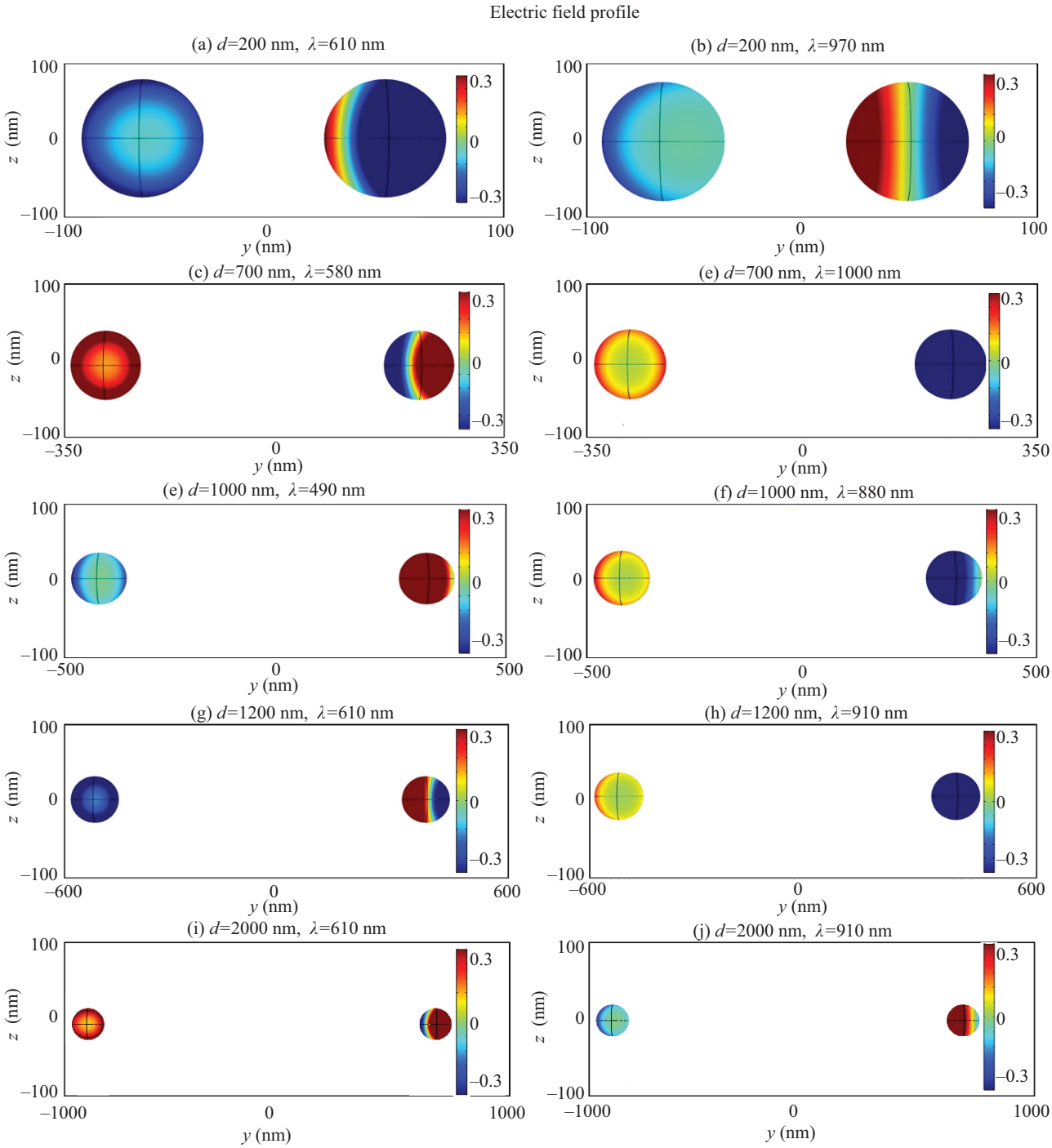


Fig. 3. (a)–(j) Electric field profiles of chiral-plasmonic nanoparticles without substrate propagating towards "$-y$" direction: (a) Inter particle gap distance $d = 200$ nm at wavelength 610 nm, (b) inter particle gap distance $d = 200$ nm at wavelength 970 nm, (c) inter particle gap distance $d = 700$ nm at wavelength 580 nm, (d) inter particle gap distance $d = 700$ nm at wavelength 1000 nm, (e) inter particle gap distance $d = 1000$ nm at wavelength 490 nm, (f) inter particle gap distance $d = 1000$ nm at wavelength 880 nm, (g) interparticle gap distance $d = 1200$ nm at wavelength 610 nm, (h) inter particle gap distance $d = 1200$ nm at wavelength 910 nm, (i) inter particle gap distance $d = 2000$ nm at wavelength 610 nm, and (j) inter particle gap distance $d = 2000$ nm at wavelength 910 nm.

Here, we observe that both the plasmonic particles and chiral nanoparticles move towards the direction of the propagation of light, hence the particles experience an optical pushing force. It is quite natural because light usually pushes any object along its propagation direction due to the momentum carried by a photon (the quanta of light).[24–27,65] The magnitude of pushing force of the chiral object is smaller than that of the plasmonic object for the near and far-field. Hence, the plasmonic nanoparticle gradually moves further away from the chiral nanoparticle by a repulsive optical binding force. The induced charges for this set-up are shown in Figs. 3(a)–3(j). According to Coulomb's law, like charges repel each other while opposite charges attract We can observe from the electric field profiles that this law plays a vital role in our study. Figures 3(a) and 3(b) show the electric field effect for the near field distance of $d = 200$ nm, while figures 3(i) and 3(j)

represent the electric field effect for the far-field distance of $d = 2000$ nm. Here in both cases, like charges are induced on the surfaces of both nanoparticles facing each other, and a repulsive longitudinal optical binding force is observed. Similarly, figures 3(c)– 3(h) show the electric field profiles against interparticle distance where plasmonic and chiral nanoparticles have the like F–F charges.

Next, for the same configuration, we change the propagation direction of light as can be seen from Fig. 1(b). In this case, the electromagnetic (EM) wave is now propagating towards the "$+y$" direction hitting the plasmonic nanoparticle first. The variation range of wavelengths remains the same as that for the previous case. Figures S3(b)–S3(d) (in supplementary materials) show the near and far-field optical binding force for this case. We observe that the plasmonic and the chiral objects experience optical pushing force which is the same as the secnario of previous set up (Fig. 1(a)). Here, the magnitude of the pushing force of plasmonic object is bigger than the chiral one, as a result, it moves towards the chiral nanoparticle gradually and the attractive optical binding force for near-field region and the far-field region are obtained. Again, no reversals of optical binding forces are observed. The electric field profiles of the plasmonic-chiral heterodimers setup are shown in Figs. S4(a)–S4(j) (in supplementary materials). Figures S4(a) and S4(b) show the electric field for near-field distance $d = 200$ nm, and figures S4(i) and S4(j) represent the electric field effect for the far-field distance $d = 2000$ nm. Here, the electric field makes the opposite charges accumulate on the chiral spheres and plasmonic spheres for the near-field region and for the far-field region and try to attract each other. Similarly, figures S4(c)–S4(h) show the electric field profiles for the other interparticle distances where plasmonic particles and chiral nanoparticles have opposite F–F charges.

So, for both cases, it can be estimated that when EM waves propagate, they produce surface plasmons on the plasmonic object, and surface plasmon resonance (SPR) takes place due to their interaction. Generally, it is estimated that plasmonic force arises from the charges induced by the surface force (due to the free electrons on the nanoparticle surface).[12,56] The characteristics of SPR of plasmonic nanospheres depend on their sizes, shapes, compositions,[12,66] and arrangements within the assemblies of nanoparticles.[12,67] We use a very small radius $r = 100$ nm for both the plasmonic dimers and the chiral hybrid dimers. Owing to this small radius of the plasmonic nanoparticle, all the electrons within the nanostructure can be easily excited and attributed to the plasmon's oscillation.[12,46] Therefore, plasmonic nanoparticles interact more strongly with the electromagnetic (EM) wave than the chiral one.[12] We can conclude from above discussion that there is a strong interaction between the nanospheres and the electric field, causing charges to accumulate on the particles.

When we place our proposed setups in an air medium, in the first case we obtain the strong repulsive force due to the presence of similar induced charges, while in the second case we observe strong attractive force due to the presence of opposite charges. However, for both these cases, we fail to obtain attractive optical binding force nor repulsive optical binding force at the same time. It is possible to control the attraction and repulsion between the particles by changing the direction of light source. However, this is not the 'direct' reversal of optical binding force. In the next subsection(s), we will figure out some possible ways of realizing the 'direct' reversal of optical binding force.

4.2. Plasmonic and chiral hybrid heterodimers with substrate: Reversal of longitudinal optical binding force at near and far-field regions

In our previous investigation, we were not able to reverse the optical binding force of plasmonic dimers and chiral heterodimers in a single configuration (without changing the propagation direction of light). However, now we are to obtain a possible solution by keeping a plasmonic substrate underneath the heterodimers. From our new configuration, we obtain the attractive optical binding force and the repulsive optical binding force in the same setup. The schematic diagrams of our proposed configurations are shown in Figs. 1(c) and 1(d).

Firstly, we simulate the configuration with an incident light which propagates in the "$+y$" direction hitting the plasmonic nanoparticle first as shown in Fig. 1(c). Figures S5(b)–S5(d) show the achieved optical binding forces by using this new arrangement for various interparticle distances. However, the repulsive binding forces are very small compared with the attractive forces. This is the drawback of this arrangement. We overcome this drawback in the next (ultimate) final set-up. The detailed physics behind the observed longitudinal binding force (when the light is hitting the plasmonic object at first) is discussed in supplementary information.

Our main aim is to obtain a strong reversal of optical binding force in both the near-field region and the far-field region for plasmonic dimers and chiral hybrid heterodimers. Although we could obtain a reversal of optical binding force in our previous setup where light propagates in the "$+y$" direction, we failed to obtain a decent repulsive force. So, to achieve our desired result, we illuminate the same setup by using a plane wave propagating towards the "$-y$" direction hitting the chiral nanoparticle first, as shown in Fig. 1(d). The

interparticle gap distances remain the same in a range from 200 nm to 2000 nm.

As shown in Figs. 4(b)–4(d), we observe the attractive optical binding forces and the repulsive optical binding forces for the cases of near field and far field when the direction of the incident light is changed to the "$-y$" direction. The magnitude of the optical binding force starts as an attractive force and gradually decreases as the wavelength of light increases until it turns into a repulsive force. Comparing with our previous configuration we obtain a strong attractive force and a strong repulsive force in our new setup, in both the near-field region and the far-field region ($d = 200$ nm to 2000 nm).

Figures 4(b) and 4(c) show the optical binding forces for distances of 200 nm, 500 nm, 700 nm, and 1000 nm respectively. In all these cases, the positive (attractive) optical binding force reverses its polarity in-between wavelengths (λ) 500 nm–600 nm and becomes negative (repulsive). As we move to even higher wavelengths ($\lambda = 1100$ nm–1200 nm) the magnitude of the negative optical binding force decreases and again becomes positive. This observation is emphasized because, in Fig. 4(d), we can see that the optical binding forces for $d = 1200$ nm and 2000 nm show a second reversal in each case.

Initially, in the attractive region, as light hits on the chiral object first, it exerts a larger optical pushing force than the plasmonic object at the lower wavelengths for the cases of near field and far field. As the magnitude of pushing force of the chiral particle is higher, the chiral particle moves toward the plasmonic nanoparticle and we obtain an attractive optical binding force. As the wavelength of the incident light increases, the magnitude of pushing force of the chiral nanoparticle decreases, and that of the plasmonic nanoparticle increases gradually. At one point the magnitude of pushing force of the plasmonic nanoparticle exceeds that of the chiral nanoparticle and the plasmonic nanoparticles undergo a stronger optical pushing force. Hence, the plasmonic particle moves away from the chiral particle. Exactly at this point, the state of the induced current profile of the plasmonic object is reversed. From Figs. 5(e), 5(g), 5(i), and 5(k) and Figs. 5(f), 5(h), 5(j), and 5(l), we can observe that the induced current on the plasmonic object is reversed for the cases of the near field and far field. Previously we saw that this reversal of current turns the optical pushing force into an optical pulling force for plasmonic object as light hits on the plasmonic object first. But in this case light hits on the chiral object first. Here, the induced current reversal of plasmonic object does not reverse the optical force (F_y) of the plasmonic, rather it enhances the force. Now for the longer wavelength, the optical pushing force of plasmonic object is larger than that of the chiral object, thus repulsion of the optical binding force occurs.

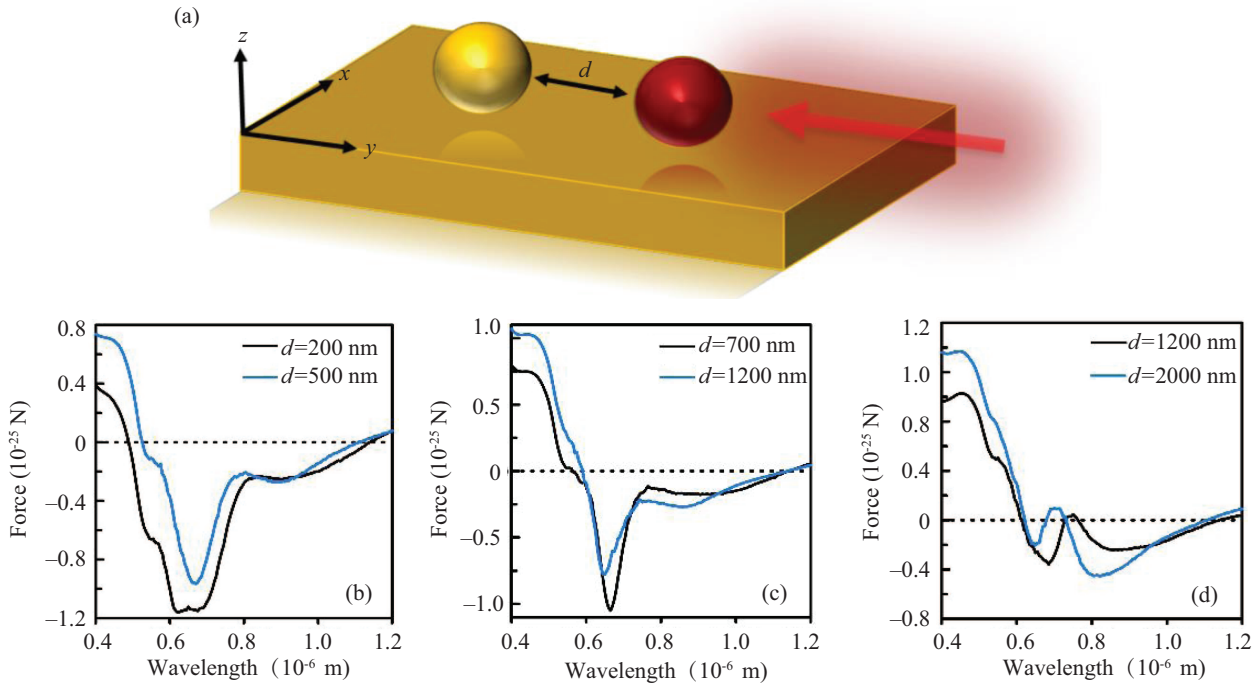


Fig. 4. The "x"-polarized plane wave propagating in the "$-y$" direction towards chiral (right) and plasmonic (left) heterodimer nanoparticles placed over a plasmonic substrate, where the spheres' inter-particle distance is d and the wavelength varies from 400 nm to 1200 nm in all cases. (a) A chiral and a plasmonic sphere (radius, $r = 100$ nm) are placed in air medium and their inter-particle gap distance is d. (b) The optical binding forces (along the "y" axis) are shown between the two hybrid dimers, for gap distance 200 nm and 500 nm by varying wavelengths. (c) Optical binding forces ($F_{\text{bind}}(y)$) are shown between the heterodimers, for gap distance 700 nm and 1000 nm by varying wavelengths. (d) Optical binding forces for the same setup for $d = 1200$ nm and 2000 nm are shown. Panels (b)–(d) show strong reversal of longitudinal optical binding forces (left sphere is plasmonic and right sphere is chiral).

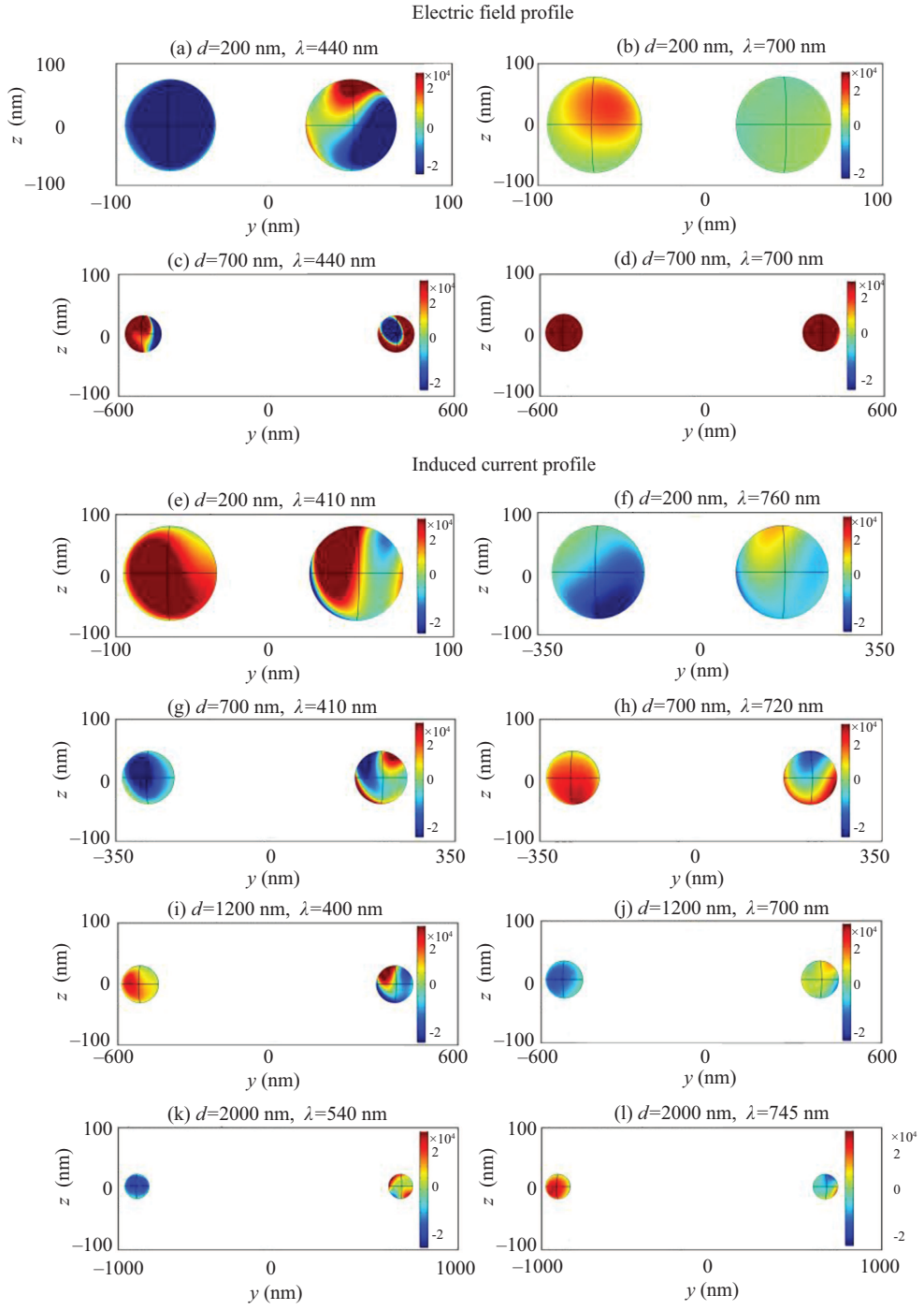


Fig. 5. (a)–(d) Electric field polarization profiles of chiral-plasmonic nanoparticles placed over a plasmonic substrate, light propagates along "$-y$" direction light hitting the chiral object first: (a) inter particle gap distance $d = 200$ nm at wavelength 440 nm, (b) inter particle gap distance $d = 200$ nm at wavelength 700 nm, (c) inter particle gap distance $d = 1200$ nm at wavelength 440 nm, (d) inter particle gap distance $d = 1200$ nm at wavelength 700 nm. Induced current profiles for plasmonic-chiral nanoparticles placed over a plasmonic substrate: (e) inter particle gap distance $d = 200$ nm at wavelength 410 nm, (f) inter particle gap distance $d = 200$ nm at wavelength 760 nm, (g) inter particle gap distance $d = 700$ nm at wavelength 410 nm, (h) inter particle gap distance $d = 700$ nm at wavelength 720 nm, (i) inter particle gap distance $d = 1200$ nm at wavelength 400 nm, (j) inter particle gap distance $d = 1200$ nm at wavelength 700 nm, (k) inter particle gap distance $d = 2000$ nm at wavelength 540 nm, and (l) inter particle gap distance $d = 2000$ nm at wavelength 745 nm.

However, behind the reversal of optical binding forces for this case, we find another phenomenon: for the longer wavelength (longer than 750 nm), the chiral object experiences optical pulling force for the cases of the near field and far field. Previously, the chiral object did not experience any pulling force in the whole wavelength range when the heterodimer setup was placed in an air medium without substrate in Fig. 2(a). We broke the environmental symmetry by placing a plasmonic substrate underneath the hybrid dimer setup and when light hits on the chiral object an optical pulling force is exerted on the chiral nanoparticle for $\lambda >$ about 750 nm. Figures 6(a)–6(f) show the current density profile for the chiral object in the near-field region and the far-field region. In this case, for the cases of near field and far field, we observe

that the chiral object experiences an optical pulling force at a wavelength of about 750 nm.

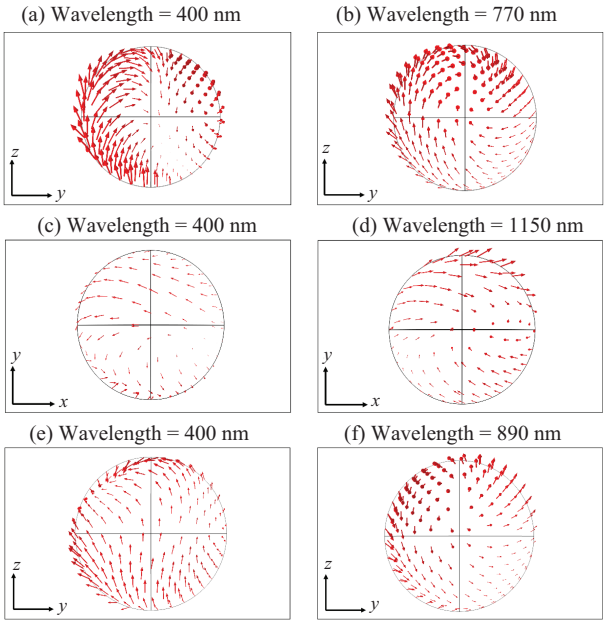


Fig. 6. (a)–(f) Induced current density profiles on chiral nanoparticles when the chiral and plasmonic nanoparticle are placed over a plasmonic substrate, light propagates along "$-y$" direction light hitting the chiral object first: (a) for inter particle gap distance $d = 200$ nm at wavelength 400 nm, (b) for inter particle gap distance $d = 200$ nm at wavelength 770 nm, (c) for inter particle gap distance $d = 700$ nm at wavelength 400 nm, (d) for inter particle gap distance $d = 700$ nm at wavelength 1150 nm, (e) for inter particle gap distance $d = 1200$ nm at wavelength 400 nm, and (f) for inter particle gap distance $d = 1200$ nm at wavelength 890 nm. Rotating pattern of current density is observed in none of panels (a), (b), and (e), but it is indeed observed in panels (b), (d), and (f)).

Figures 6(a) and 6(b) represent the current density profile for interparticle distance, $d = 200$ nm, Figs. 6(c) and 6(d) for $d = 700$ nm and Figs. 6(e) and 6(f) for $d = 1200$ nm. Magnetic-type resonance is induced on the chiral object as indicated by a rotating pattern of current density separately in Figs. 6(b), 6(d), and 6(f). When the chiral object experiences an optical pushing force, magnetic-type resonance is not noticed on the chiral object as shown in Figs. 6(a), 6(c), and 6(e). We do not observe this rotating pattern of the current density profile of chiral objects in Fig. 6(a), nor Fig. 6(c), nor Fig. 6(e). We also study the current density profile on the chiral object when no substrate is placed underneath the background to ascertain the substrate effect. In Fig. S12, we can see that current density vector of chiral object (without substrate) is not showing any rotating pattern for longer wavelength nor shorter wavelength (see Figs. S12(a) and S12(b)). As a result, no magnetictype resonance is created on the chiral object without substrate. On the other hand, when we place a substrate underneath the particles, the current density vector of the chiral object shows rotating pattern for longer wavelength (see Figs. S12(c) and S12(d)). Thus, magnetic-type resonance is created on the chiral object. So, it can be said that the induced magnetic-type resonance on chiral object is mainly responsible for the optical pulling force on the chiral nanoparticle. Thus, a very strong repulsive optical binding force occurs between the chiral and plasmonic heterodimer setup when light hits on the chiral object first. Comparing with our last configuration, after changing the direction of the light into "$-y$" direction, we obtain a strong repulsive force. The observations of our new setup are further confirmed from the electric field profiles shown in Figs. 5(a)–5(d). These figures depict the F–F charge distribution of the heterodimers for the interparticle distances $d = 200$ nm and $d = 2000$ nm. We obtain a similar attractive force at the shorter wavelengths to earlier and to that at greater wavelengths of light; we observe a stronger repulsive force than that in our last configuration (for near and far-field). All other interparticle distances also show similar observations in their electric field profiles.

We can conclude that in the shorter wavelengths, a chiral nanoparticle experiences an optical pushing force of higher magnitude than the force on a plasmonic particle. However, with the increase of wavelength, the plasmonic nanoparticle experiences a stronger force thereby changing the overall attractive F_{bind} force into repulsive F_{bind}. Thus, we obtain a 'direct' reversal of optical binding force in the presence of a plasmonic substrate.

4.3. Chiral and plasmonic hybrid tetramers over plasmonic substrate: Reversal of lateral optical binding force in near-field region and far-field region

After we find a reversal of longitudinal optical binding force for chiral-plasmonic heterodimers, we study the idea of reversal of the near and far-field lateral optical binding force of chiral-plasmonic tetramers. Hence, we place two chiral nanoparticles and two plasmonic nanoparticles over a plasmonic (gold) substrate in an air medium as shown in Fig. 7(a). Figure 7(b) shows the same setup from a top view. This time, the layout is illuminated from above by a circularly polarized plane wave propagating in the "$-z$" direction. As we mentioned earlier, the circular polarization of light gives a more conclusive result than linearly polarized light to control the reversal of the near-field and far-field lateral optical binding force for tetramers.[48] Throughout the simulations, we have varied the wavelength of the light and increased the interparticle distances, d_x (along the "x" axis) and d_y (along the "y" axis) of the tetramers to look into the lateral binding force of the near-field region and far-field region.

Circular polarization is of two types: left-handed circularly polarized (LHCP) state and right-handed circularly polarized (RHCP) states[48] For these simulations, both forms of polarization have been used, and figures 7(c)–7(f) show the optical binding forces experienced by the tetramers in both states. We investigate the optical binding force between tetramers, both along the "x" axis ($F_{\text{bind}(x)}$) and along the "y"

axis ($F_{\text{bind}(y)}$, for LHCP and RHCP, covering interparticle distances for the near-field region and the far-field region over a wide range of wavelengths. Figures 7(c) and 7(d) show $F_{\text{bind}(x)}$ and figures 7(e) and 7(f) show $F_{\text{bind}(y)}$ for LHCP state and RHCP state. In both cases, we obtain the reversal of optical binding force for near-field region and far-field region. Throughout the whole simulations, we keep the interparticle distances (for both d_x and d_y at 200 nm, 500 nm, 700 nm, and 1000 nm, respectively.

Figures 8(a) and 8(d) show the electric field profiles of the chiral-plasmonic tetramer setup for the LHCP state of plane wave. These figures depict the face-to-face (F–F) charge distributions of the tetramers set. Figures 8(a) and 8(b) show the electric field profile for the near-field region distance $d = 200$ nm. In a shorter wavelength range, we observe like charges on the surface of the heterodimers which depict the repulsive optical binding force between the tetramers. As we move to longer wavelength opposite charges accumulate on the spheres and we observe an attractive optical binding force. Next, figures 8(c) and 8(d) represent the electric field profiles for the far-field distance $d = 700$ nm, which shows similar attraction and repulsion from shorter to longer wavelength. Again, figures 8(e)–8(h) show the electric field profiles of the chiral-plasmonic tetramer setup (as shown in Fig. 7(a) and 7(b) for the RHCP state of plane wave. Like what we can observe in Figs. 8(a)–8(d), we also find similar attraction and repulsion of charges in this case. Hence, we obtain a reversal of optical binding force in each of the two cases.

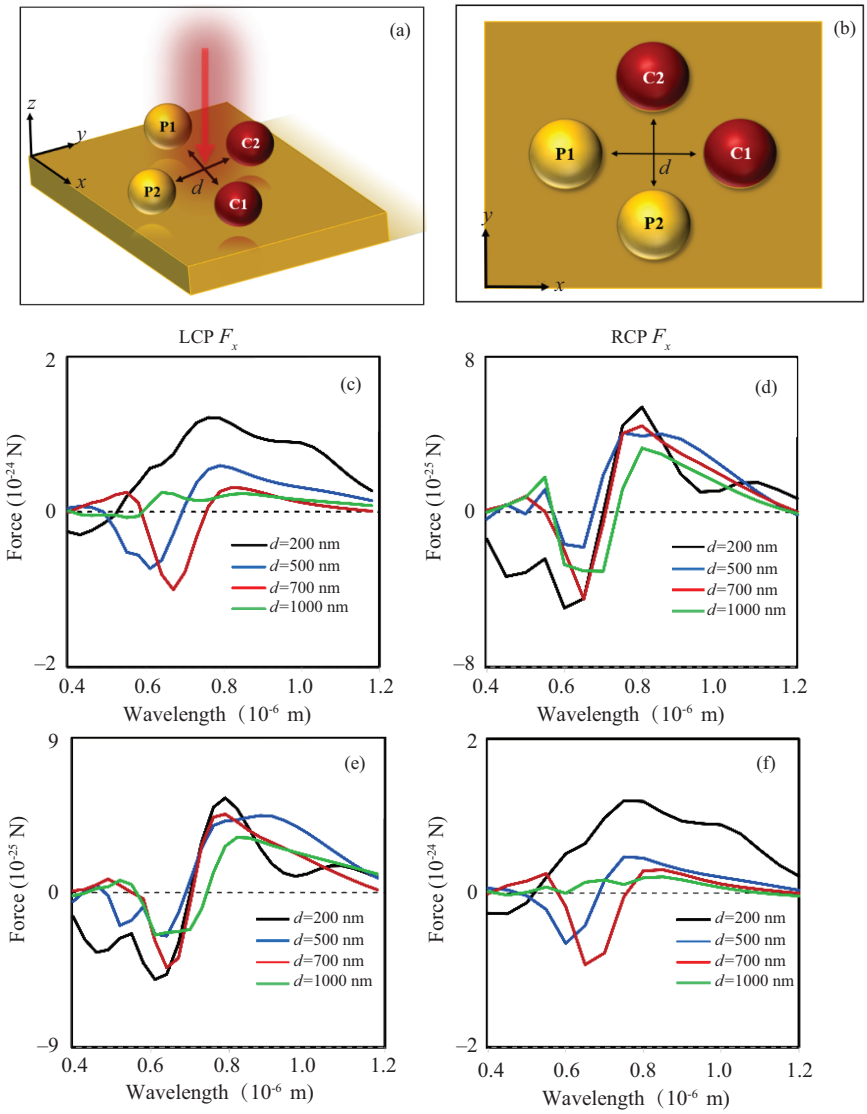


Fig. 7. (a) Circularly polarized light propagating toward "$-z$" direction among equidistant chiral-plasmonic tetramers (two chiral nanoparticles in maroon color and two plasmonic nanoparticles in gold color, interparticle distances d, placed over a plasmonic substrate); (b) the same chiral-plasmonic tetramers setup as those in panel (a), shown in top view along the "x" and "y" axes. Panels (c)–(f) show the optical binding forces for the tetramers setup for left circular polarization (LCP) and right circular polarization (RCP) along the "x" axis (F_x) and "y" axis (F_y) for wavelengths ranging from 400 nm to 1200 nm, (c) F_x of LCP for interparticle distances $d_x = 200$ nm, 500 nm, 700 nm, and 1000 nm respectively; (d) F_x of RCP for interparticle distances $d_x = 200$ nm, 500 nm, 700 nm, and 1000 nm respectively; (e) F_y of LCP for interparticle distances $d_y = 200$ nm, 500 nm, 700 nm, and 1000 nm respectively; (f) F_y of RCP for interparticle distances $d_y = 200$ nm, 500 nm, 700 nm, and 1000 nm respectively.

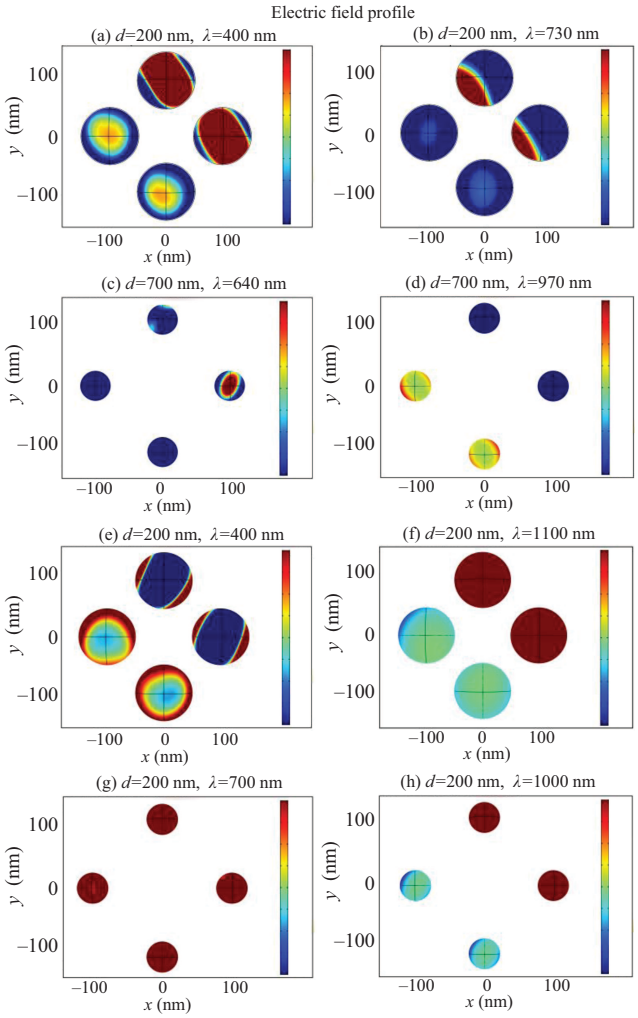


Fig. 8. Electric field profiles of chiral-plasmonic tetramers placed over a plasmonic substrate for the LHCP state of plane wave: (a) interparticle gap distance $d = 200$ nm at wavelength 400 nm, (b) interparticle gap distance $d = 200$ nm at wavelength 730 nm, (c) interparticle gap distance $d = 700$ nm at wavelength 640 nm, and (d) interparticle gap distance $d = 700$ nm at wavelength 970 nm. Electric field profiles of chiral-plasmonic tetramers placed over a plasmonic substrate for the RHCP state of plane wave: (e) interparticle gap distance $d = 200$ nm at wavelength 400 nm, (f) interparticle gap distance $d = 200$ nm at wavelength 1100 nm, (g) interparticle gap distance $d = 700$ nm at wavelength 700 nm, and (h) interparticle gap distance $d = 700$ nm at wavelength 1000 nm.

As we have mentioned earlier, the induced charges accumulate on the surface of the chiral nanoparticles and plasmonic nanoparticles when they interact with EM wave. In the near-field region, this strong interaction leads the similar charges to accumulate on the surfaces of the nanospheres facing each other at shorter wavelengths hence resulting in F–F repulsive optical binding force. Again, at longer wavelengths in the same near-field region, the opposite charges accumulate on the surfaces of the chiral-plasmonic tetramers facing each other along the two axes. The opposite charges attract each other resulting in attractive optical binding forces.

On the other hand, from the earlier researches we already know that the induced forces of the plasmonic nanospheres are much stronger than those of chiral nanospheres due to plasmonic particles' much stronger interactions with the EM wave. Therefore, the plasmonic nanoparticles' forces dominate over the chiral nanospheres' total optical binding force. The effect of the plasmonic nanoparticles' force is strong enough to convert attractive F_{bind} forces into repulsive forces in the near-field region, resulting in a reversal of optical binding force for the proposed tetramers setup. Therefore, we can conclude that the near and far-field optical binding force characteristics of chiral and plasmonic tetramers, when placed on the top of a plasmonic substrate under circularly polarized wave illumination, exhibit a reversal of lateral optical binding force.

5. Conclusions

As far as we know, no work has been reported on the reversal of longitudinal optical binding force for chiral and plasmonic hybrid dimers, neither has the reversal of lateral optical binding force for chiral and plasmonic tetramer layout. In this work, we display that when we place a plasmonic-chiral hybrid dimer set over a plasmonic substrate and illuminate it by using a linearly polarized plane wave either from the "$-y$" direction coming into contact with the chiral nanoparticle first or the "$+y$" direction hitting on the plasmonic nanoparticle first, we observe a reversal of longitudinal optical binding force. We also demonstrate that if we place chiral-plasmonic tetramers over a plasmonic substrate and cast a circularly polarized light on them from the top, we can observe a reversal of lateral optical binding force. In both cases, the reversal has been observed for the near-field region and far-field region in a wide range of wavelengths of light. Such 'direct' reversals of optical binding force the longitudinal and lateral do not occur when the dimer set-up or the tetramer set-up is placed in an air medium. The plasmonic chip underneath the particles plays a vital role in achieving such reversals longitudinal and lateral of optical binding force. As most of the biological particles are chiral in nature, the broadband reversal of optical binding force of chiral and plasmonic hybrid dimer and tetramer set can be an emerging fascinating area of optical manipulation; which can be used as a dominant instrument to accurately control the mutual attraction and repulsion for colloidal self-assembly, crystallization, and so on.

References

[1] Ashkin A 1970 *Phys. Rev. Lett.* **24** 156
[2] Greiner M, Mandel O, Esslinger T, Hänsch T W and Bloch I 2002 *Nature* **415** 39
[3] Deniz A A, Mukhopadhyay S and Lemke E A 2008 *J. Roy. Soc. Interface* **5** 15
[4] Rodríguez J, Dávila Romero L C and Andrews D L 2008 *Phys. Rev. A* **78** 043805
[5] Wang S B and Chan C T 2014 *Nat. Commun.* **5** 1
[6] Ashkin A and Dziedzic J M 1987 *Science* **235** 1517
[7] Gao D, Ding W, Nieto-Vesperinas M, Ding X, Rahman M, Zhang T, Lim C T and Qiu C W 2017 *Light: Science and Applications* **6** e17039
[8] Dienerowitz M, Mazilu M and Dholakia K 2008 *J Nanophoton.* **2** 021875

[9] Neuman K C and Nagy A 2008 *Nat. Methods* **5** 491
[10] Burns M M, Fournier J M and Golovchenko J A 1989 *Phys. Rev. Lett.* **63** 1233
[11] Rivy H M, Mahdy M R C, Masud N, Jony Z R and Das S C 2020 *Commun. Theor. Phys.* **72** 045502
[12] Ahsan N B, Shamim R, Mahdy M R C, Das S C, Rivy H M, Dolon C I, Hossain M and Faisal K M 2020 *J. Opt. Soc. Am. B* **37** 1273
[13] Andrews D L, Crisp R G and Bradshaw D S 2006 *J. Phys. B: At. Mol. Opt. Phys.* **39** S637
[14] Grzegorczyk T M, Kemp B A and Kong J A 2006 *Opt. Lett.* **31** 3378
[15] Grzegorczyk T M, Kemp B A and Kong J A 2006 *Phys. Rev. Lett.* **96** 113903
[16] Karásek V, Dholakia K and Zemánek P 2006 *Appl. Phys. B* **84** 149
[17] Guillon M, Moine O and Stout B 2006 *Phys. Rev. Lett.* **96** 143902
[18] Metzger N K, Marchington R F, Mazilu M, Smith R L, Dholakia K and Wright E M 2007 *Phys. Rev. Lett.* **98** 068102
[19] Ahlawat S, Dasgupta R and Gupta P K 2007 *Proc. SPIE* (*Saratov: Optical Technologies in Biophysics and Medicine VIII*) 65350W
[20] Karásek V and Zemánek P 2007 *J. Opt.* **9** S215
[21] Andrews D L 2008 *Structures light and its applications: An introduction to phase-structured beams and nanoscale optical forces* (Massachusetts: Academic Press) pp. 12–56, 82–129
[22] Guillon M and Stout B 2008 *Phys. Rev. A* **77** 023806
[23] Li M and Arlt J 2008 *Opt. Commun.* **281** 135
[24] Marchington R F, Mazilu M, Kuriakose S, Garcés-Chávez V, Reece P J, Krauss T F, Gu M and Dholakia K 2008 *Opt. Express* **16** 3712
[25] Mohanty S K, Andrews J T and Gupta P K 2004 *Opt. Express* **12** 2746
[26] Mellor C D, Fennerty T A and Bain C D 2006 *Opt. Express* **14** 10079
[27] Burns M M, Fournier J M and Golovchenko J A 1990 *Science* **249** 749
[28] Rivy H M, Mahdy M R C, Jony Z R, Masud N, Satter S S and Jani R 2019 *Opt. Commun.* **430** 51
[29] Novitsky A, Qiu C W and Wang H 2011 *Phys. Rev. Lett.* **107** 203601
[30] Chen J, Ng J, Lin Z and Chan C T 2011 *Nat. Photon.* **5** 531
[31] Zhu T, Cao Y, Wang L, Nie Z, Cao T, Sun F, Jiang Z, Nieto-Vesperinas M, Liu Y, Qiu C W and Ding W 2018 *Phys. Rev. Lett.* **120** 123901
[32] Ruffner D B and Grier D G 2012 *Phys. Rev. Lett.* **109** 163903
[33] Zhang T, Mahdy M R C, Liu Y, Teng J H, Lim C T, Wang Z and Qiu C W 2017 *ACS Nano* **11** 4292
[34] Zhang Q, Li J and Liu X 2019 *Phys. Chem. Chem. Phys.* **21** 1
[35] Rodríguez-Fortunõ F J, Engheta N, Martínez A and Zayats A V 2015 *Nat. Commun.* **6** 8799
[36] Ashkin A, Dziedzic J M and Yamane T 1987 *Nature* **330** 769
[37] Tang Y and Cohen A E 2010 *Phys. Rev. Lett.* **104** 163901
[38] Zhang S, Park Y S, Li J, Lu X, Zhang W and Zhang X 2009 *Phys. Rev. Lett.* **102** 023901
[39] Wang B, Zhou J, Koschny T, Kafesaki M and Soukoulis C M 2009 *J. Opt. A* **11** 114003
[40] Brown L V, Sobhani H, Lassiter J B, Nordlander P and Halas N J 2010 *ACS Nano* **4** 819
[41] Aćimović S S, Kreuzer M P, González M U and Quidant R 2009 *ACS Nano* **3** 1231 2009 *ACS Nano* **3** 1231
[42] Miljković V D, Pakizeh T, Sepulvda B, Johansson P and Käll M 2010 *J. Phys. Chem. C* **114** 7472
[43] Zhang Q, Xiao J J, Zhang X M, Yao Y and Liu H 2013 *Opt. Express* **21** 6601
[44] Zhang Q and Xiao J J 2013 *Opt. Lett.* **38** 4240
[45] Mahdy M R C, Zhang T, Danesh M and Ding W 2017 *Sci. Rep.* **7** 1
[46] Liu H, Ng J, Wang S B, Hang Z H, Chan C T and Zhu S N 2011 *New J. Phys.* **13** 073040
[47] Mahdy M R C, Danesh M, Zhang T, Ding W, Rivy H M, Chowdhury A B and Mehmood M Q 2018 *Sci. Rep.* **8** 3164
[48] Satter S S, Mahdy M R C, Ohi M A R, Islam F and Rivy H M 2018 *J. Phys. Chem. C* **122** 20923
[49] Bradshaw D S, Forbes K A, Leeder J M and Andrews D L 2015 *Photonics* **2** 483
[50] Chen H, Jiang Y, Wang N, Lu W, Liu S and Lin Z 2015 *Opt. Lett.* **40** 5530
[51] Forbes K A and Andrews D L 2015 *Phys. Rev. A* **91** 053824
[52] A Salam 2015 *AIP Conference Proceedings* **1642** 90
[53] Zhu Y, Wu Z, Li Z and Shang Q 2015 *Procedia Engineering* **102** 329
[54] Forbes K A, Bradshaw D S and Andrews D L 2020 *Nanophotonics* **9** 1
[55] Min C, Shen Z, Shen J, Zhang Y, Fang H, Yuan G, Du L, Zhu S, Lei T and Yuan X 2013 *Nat. Commun.* **4** 2891
[56] Raziman T V and Martin O J F 2015 *Opt. Express* **23** 20143
[57] Zhao X, Zang S Q and Chen X 2020 *Chem. Soci. Rev.* **49** 2481
[58] Burke D and Henderson D J 2002 *British J. Anaesthesia* **88** 563
[59] Nguyen L A, He H and Pham-Huy C 2006 *Int. J. Biomed. Sci.* **2** 85
[60] Qiu C W, Ding W, Mahdy M R C, Gao D, Zhang T, Cheong F C, Dogariu A, Wang Z and Lim C T 2015 *Light: Science and Applications* **4** e278
[61] Kemp B A 2011 *J. Appl. Phys.* **109** 111101
[62] Baxter C and Loudon R 2010 *J. Mod. Opt.* **57** 830
[63] Bohren C F and Huffman D R 2013 *Absorption and Scattering of Light by Small Particles* (New York: Wiley) pp. 57–81, 82–129
[64] Lakhtakia A, Varadan V K and Vasundara V 1989 *Time-Harmonic Electromagnetic Fields in Chiral Media* (Berlin: Springer) Vol. 335, pp. 5–13
[65] Dogariu A, Sukhov S and Sáenz J 2013 *Nat. Photon.* **7** 24
[66] Wang X, Zou Y, Zhu J and Wang Y 2013 *J. Phys. Chem. C* **117** 14197
[67] Bishop K J M, Wilmer C E, Soh S and Grzybowski B A 2009 *Small* **5** 1600